Supplement of Atmos. Chem. Phys., 22, 12153–12166, 2022
https://doi.org/10.5194/acp-22-12153-2022-supplement

Atmospheric Chemistry and Physics
Open Access
EGU

Supplement of

Chemical characteristics and sources of $PM_{2.5}$ in Hohhot, a semi-arid city in northern China: insight from the COVID-19 lockdown

Haijun Zhou et al.

Correspondence to: Haijun Zhou (hjzhou@imnu.edu.cn)

Table S1. Summary of error estimation diagnostics from BS and DISP over the sampling year

BS Mapping	CC	BB	CD	SIAs	VE	CS	Unmapped
CC	100	0	0	0	0	0	0
BB	0	86	0	8	6	0	0
CD	0	0	100	0	0	0	0
SIAs	0	0	0	100	0	0	0
VE	0	0	0	0	100	0	0
CS	0	0	0	4	0	96	0
DISP Diagnostics							
Error Code:	0						
Largest Decrease in Q:	-0.042						
%dQ:	-0.0003						
Swaps by Factor:	0	0	0	0	0	0	

CC, VE, CS, CD, SIAs, and BB represent coal combustion, vehicular emission, crustal source, construction dust, secondary inorganic aerosols, and biomass burning, respectively.

Table S2. Summary of error estimation diagnostics from BS and DISP in spring

BS Mapping	VE	CD	SIAs	CS	CC	BB	Unmapped
VE	96	2	1	0	1	0	0
CD	2	98	0	0	0	0	0
SIAs	0	0	100	0	0	0	0
CS	0	0	0	100	0	0	0
CC	0	0	0	0	100	0	0
BB	0	0	0	0	0	100	0
DISP Diagnostics							
Error Code:	0						
Largest Decrease in Q:	-0.0430						
%dQ:	-0.0017						
Swaps by Factor:	0	0	0	0	0	0	

CC, VE, CS, CD, SIAs, and BB represent coal combustion, vehicular emission, crustal source, construction dust, secondary inorganic aerosols, and biomass burning, respectively.

Table S3. Summary of error estimation diagnostics from BS and DISP in summer

BS Mapping	SIAs	Unknown	CS	BB	VE	CC	Unmapped
SIAs	100	0	0	0	0	0	0
Unknown	0	98	0	0	2	0	0
CS	1	1	95	0	3	0	0
BB	1	0	0	87	10	1	1
VE	2	0	0	0	95	3	0
CC	5	0	0	0	1	94	0
DISP Diagnostics							
Error Code:	0						
Largest Decrease in Q:	-0.1070						
%dQ:	-0.0045						
Swaps by Factor:	0	0	0	0	0	0	

CC, VE, CS, CD, SIAs, and BB represent coal combustion, vehicular emission, crustal source, construction dust, secondary inorganic aerosols, and biomass burning, respectively.

Table S4. Summary of error estimation diagnostics from BS and DISP in autumn

BS Mapping	CD	CC	SIAs	BB	CS	VE	Unmapped
CD	100	0	0	0	0	0	0
CC	1	99	0	0	0	0	0
SIAs	0	0	100	0	0	0	0
BB	2	1	3	90	2	1	1
CS	0	2	0	0	96	2	0
VE	0	0	0	0	0	100	0
DISP Diagnostics							
Error Code:	0						
Largest Decrease in Q:	-0.3860						
%dQ:	-0.0109						
Swaps by Factor:	0	0	0	0	0	0	

CC, VE, CS, CD, SIAs, and BB represent coal combustion, vehicular emission, crustal source, construction dust, secondary inorganic aerosols, and biomass burning, respectively.

Table S5. Summary of error estimation diagnostics from BS and DISP in winter

BS Mapping	BB	SIAs	CS	CC	CD	VE	Unmapped
BB	93	1	0	3	1	2	0
SIAs	0	100	0	0	0	0	0
CS	0	0	100	0	0	0	0
CC	0	0	0	100	0	0	0
CD	0	0	0	3	90	7	0
VE	0	0	0	0	0	100	0
DISP Diagnostics							
Error Code:	0						
Largest Decrease in Q:	-0.0400						
%dQ:	-0.0017						
Swaps by Factor:	0	0	0	0	0	0	

CC, VE, CS, CD, SIAs, and BB represent coal combustion, vehicular emission, crustal source, construction dust, secondary inorganic aerosols, and biomass burning, respectively.

Table S6. Summary of error estimation diagnostics from BS and DISP during pre-LD

BS Mapping	CD	CC	SIAs	VE	CS	Unmapped
CD	95	1	1	0	2	1
CC	2	96	0	1	1	0
SIAs	3	0	97	0	0	0
VE	1	5	3	91	0	0
CS	2	2	0	0	96	0
DISP Diagnostics						
Error Code:	0					
Largest Decrease in Q:	-0.0810					
%dQ:	-0.0111					
Swaps by Factor:	0	0	0	0	0	

CC, VE, CS, CD, SIAs, and BB represent coal combustion, vehicular emission, crustal source, construction dust, secondary inorganic aerosols, and biomass burning, respectively.

Table S7. Summary of error estimation diagnostics from BS and DISP during LD

BS Mapping	CD	CC	SIAs	VE	BB	CS	Unmapped
CD	99	0	0	1	0	0	0
CC	0	99	0	0	0	1	0
SIAs	0	0	99	1	0	0	0
VE	0	11	0	89	0	0	0
BB	0	0	3	0	97	0	0
CS	0	9	0	2	0	89	0
DISP Diagnostics							
Error Code:	0						
Largest Decrease in Q:	-0.0490						
%dQ:	-0.0119						
Swaps by Factor:	0	0	0	0	0	0	

CC, VE, CS, CD, SIAs, and BB represent coal combustion, vehicular emission, crustal source, construction dust, secondary inorganic aerosols, and biomass burning, respectively.

Table S8. Summary of error estimation diagnostics from BS and DISP during post-LD

BS Mapping	CC	VE	SIAs	BB	CS	Unmapped
CC	100	0	0	0	0	0
VE	0	97	0	1	2	0
SIAs	0	0	100	0	0	0
BB	0	0	0	100	0	0
CS	3	0	1	0	95	1
DISP Diagnostics						
Error Code:	0					
Largest Decrease in Q:	-0.1500					
%dQ:	-0.0087					
Swaps by Factor:	0	0	0	0	0	0

CC, VE, CS, CD, SIAs, and BB represent coal combustion, vehicular emission, crustal source, construction dust, secondary inorganic aerosols, and biomass burning, respectively.

Table S9. Comparison of chemical composition of $PM_{2.5}$ in Hohhot and other cities.

Location	Date type	period	$PM_{2.5}$ ($\mu g\ m^{-3}$)	Percentage (%)								Reference
				OM	SO_4^{2-}	NO_3^-	NH_4^+	Cl^-	EC	MD	others	
Hohhot	Offline	pre-LD	108.7	27.8	24.4	22.9	8.0	2.9	4.6	4.7	4.7	This study
		LD	68.3	30.5	17.2	18.0	4.9	3.9	5.4	11.8	8.2	
		post-LD	32.6	35.0	9.5	10.2	1.8	2.8	7.5	18.9	14.2	
		anuual	42.6	31.5	13.4	12.3	3.3	2.5	6.6	14.2	16.1	
Xi'an	online	pre-LD	102.0	42	7	30	13	3	-	-	8	(Tian et al., 2021)
		LD	60.2	48	8	25	12	3	-	-	7	
Tianjin	online	LD	-	10.6	9.8	20.2	9.7	2.8	3.1	-	43.8	(Ding et al., 2021)
		Same period in 2019	-	13.7	8.3	14.5	8.2	4.0	3.6	-	47.7	
Guangzhou	online	pre-LD	-	18.2[a]	19.5	37.8	21.4	-	3.1	-	-	(Wang et al., 2021)
		LD	-	35.2[a]	20.3	18.7	22.1	-	3.8	-	-	
Beijing	online	pre-LD	32.2	18.3	12.1	22.2	14.2	3.6	3.0	-	26.5[c]	(Ren et al., 2021)
		LD	50.0	15.8	16.1	26.1	16.1	3.0	2.6	-	20.4[c]	
Nanjing	online	pre-LD	68.2	12.3	18.0	34.4	15.8	1.9	2.5	-	15.3[c]	
		LD	44.0	17.9	21.5	24.7	14.1	3.2	1.9	-	16.8[c]	
Changsha	online	pre-LD	59.6	16.8	11.3	26.7	12.7	1.2	2.2	-	29.0[c]	
		LD	36.6	20.8	12.5	14.2	9.2	1.5	1.3	-	40.5[c]	
Shanghai	online	pre-LD	60.9	23.5[b]	18.6	37.5	19.3	1.2	-	-	-	(Chen et al., 2020)
		LD	41.2	39.5[b]	21.0	29.4	18.4	1.7	-	-	-	
		post-LD	34.0	25.5[b]	27.4	26.6	19.1	1.5	-	-	-	

[a] The sum of POC and SOC. [b] Sum of oxygenated and hydrocarbon-like organic aerosols. [c] Sum of trace elements and unidentified. "-" represent no date available in the reference. Pre-LD, LD, and post-LD represent pre-lockdown, lockdown, and post-lockdown period, respectively.

Table S10 The changes of chemical composition of $PM_{2.5}$ in Hohhot during pre-LD, LD, post-LD

species	period	Concentration		Percentage	
		change (μg m^{-3})	p	Change (%)	p
SO_4^{2-}	LD	-12.42	0.004	-7.02	0.055
	post-LD	-17.46	0.000	-11.36	0.003
NO_3^-	LD	-10.38	0.007	-4.75	0.210
	post-LD	-13.41	0.001	-8.23	0.036
NH_4^+	LD	-4.27	0.005	-3.04	0.032
	post-LD	-5.41	0.001	-4.44	0.003
Cl-	LD	-0.81	0.129	+0.96	0.154
	post-LD	-1.71	0.002	-0.14	0.841
OM	LD	-9.51	0.000	+2.35	0.423
	post-LD	-17.55	0.000	+2.97	0.326
EC	LD	-1.53	0.000	+0.79	0.276
	post-LD	-2.27	0.000	+2.07	0.006
MD	LD	+1.89	0.187	+6.96	0.003
	post-LD	+0.51	0.726	+11.55	0.000

Pre-LD, LD, and post-LD represent pre-lockdown, lockdown, and post-lockdown period, respectively. "-" and "+" represent "decrease" and "increase", respectively.

Table S11. Comparison of source contribution of $PM_{2.5}$ in Hohhot during pre-LD, LD, post-LD, and over the sampling year.

Location	Date type	Model	$PM_{2.5}$ ($\mu g\ m^{-3}$)	Source contribution (%)							Reference
				period	CC	VE	DS	SIAs	BB	SS	IP	
Hohhot	Offline	PMF	108.7	pre-LD	32.2	35.5	11.2[a]	21.1	-	-	-	This study
			68.3	LD	30.5	4.4	18.0[a]	37.8	9.4	-	-	
			32.6	post-LD	68.7	14.7	10.6[a]	5.0	-	-	-	
Tangshan	Online	PMF	-	pre-LD	12	-	4	36	21	-	27	(Wang et al., 2021)
			-	LD	9	-	7	44	20	-	20	
Taiyuan	online	PMF	122.0	pre-LD	5.5	23.1	4.0	62.0	-	-	3.5	(Yumin et al., 2021)
			83.3	LD	6.2	7.7	2.3	71.5	-	-	3.4	
Xiamen	online	PMF	46.2	pre-LD	9	33	13	27	-	4	12	(Hong et al., 2021)
			24.4	LD	33	24	4.5	31	-	3	4	
			32.4	post-LD	11	25	24	25	-	8	7	
Hohhot	Offline	PMF	32.4	Spring	56.1	17.0	22.6[a]	4.2	-	-	-	This study
			24.3	Summer	24.0	48.4	19.7[a]	5.3	2.6	-	-	
			37.0	autumn	38.9	33.8	16.1[a]	11.1	-	-	-	
			80.8	winter	65.4	14.3	6.8[a]	10.5	-	-	-	
			42.6	annual	38.3	35.0	13.5[a]	11.4	1.7	-	-	
Tianjin	Offline	PMF	60.1	annual	25	21	7	30	-	2[b]	5	(Tian et al., 2021)
	Online	PMF	54.3	annual	24	18	4	38	-	1[b]	4	
Shanghai	Offline	PMF	73.7	annual	2.4	18.3	4.6	31.6	12.3	10.6[c]	20.2	(Feng et al., 2022)
Beijing	Offline	PMF	-	annual	11.1	24.7	4.3	48.1[d]	11.7	-	-	(Z ƙov á et al., 2016)

CC, VE, DS, SIAs, BB, SS, IP represent coal combustion, vehicular emission, dust source, secondary inorganic aerosols, biomass burning, sea salt, and industrial process, respectively. "-" represent no date available in the reference. [a] Sum of CS and CD contributions in this study. [b] Sum of SS and BB. [c] Ship emission. [d] Sum of secondary sulfate and secondary nitrate. Pre-LD, LD, and post-LD represent pre-lockdown, lockdown, and post-lockdown period, respectively.

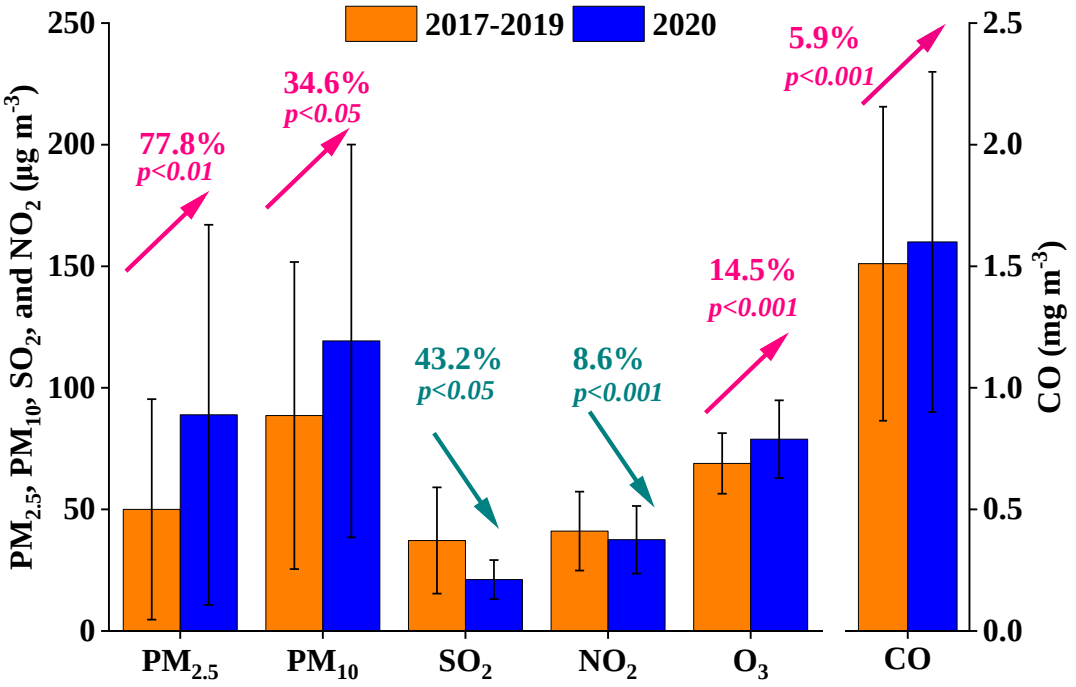

Figure S1. Comparison of air pollutants in Hohhot during the LD period with the same period in 2017-2019.

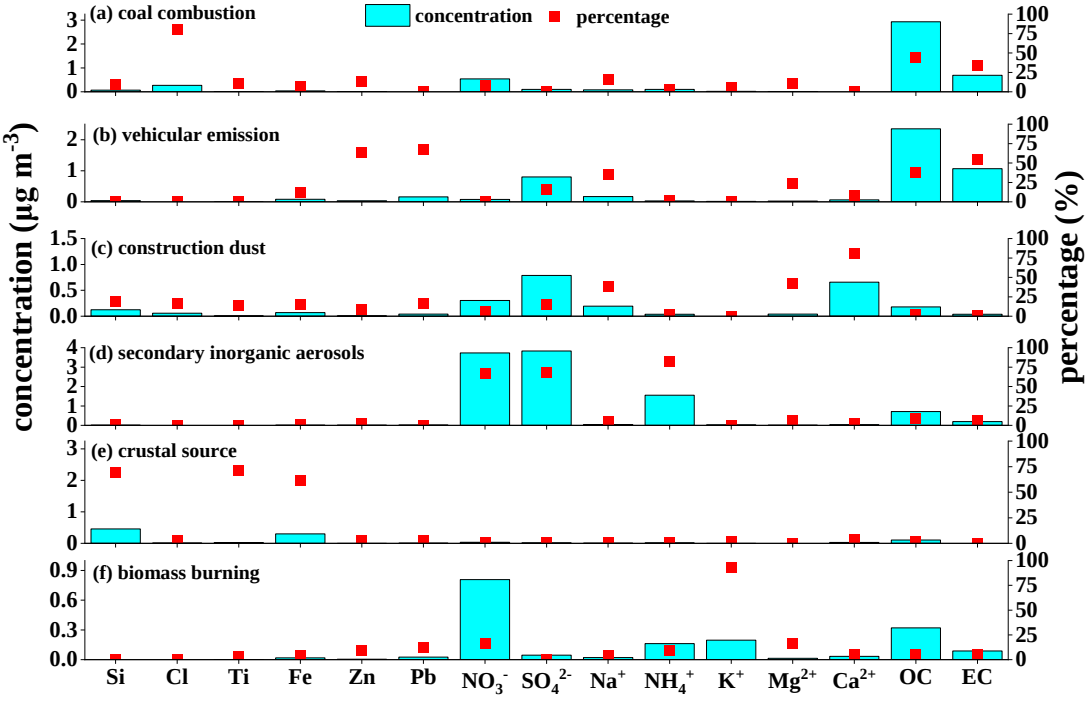

Figure S2. Source profiles of PMF for the whole sampling year.

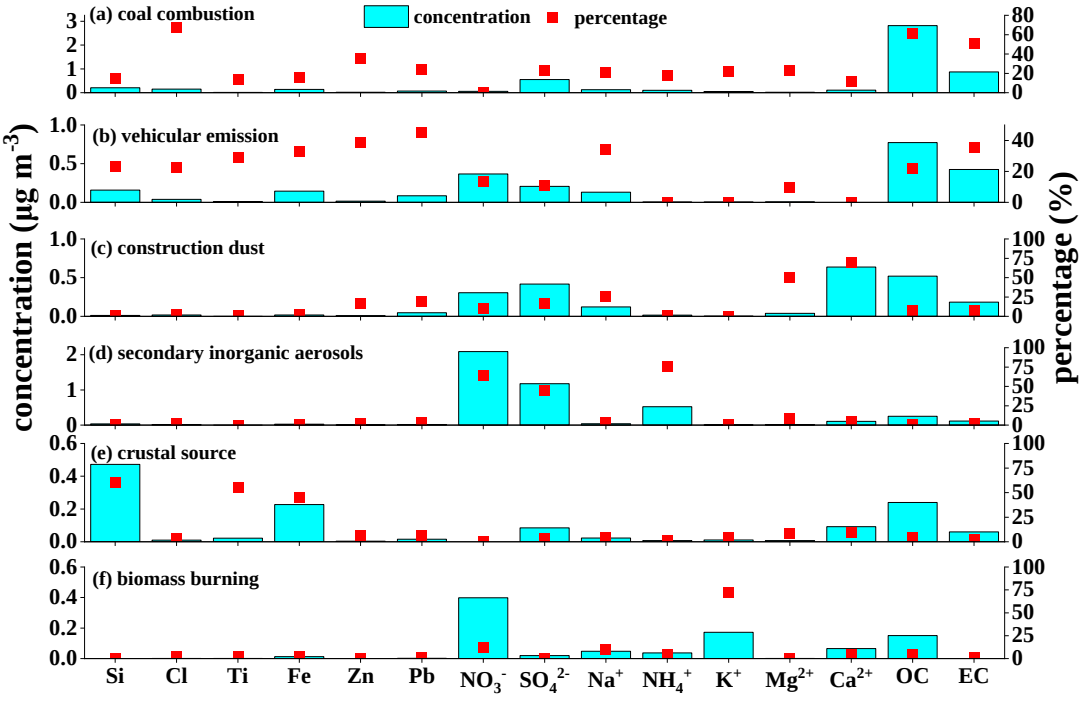

Figure S3. Source profiles of PMF for spring.

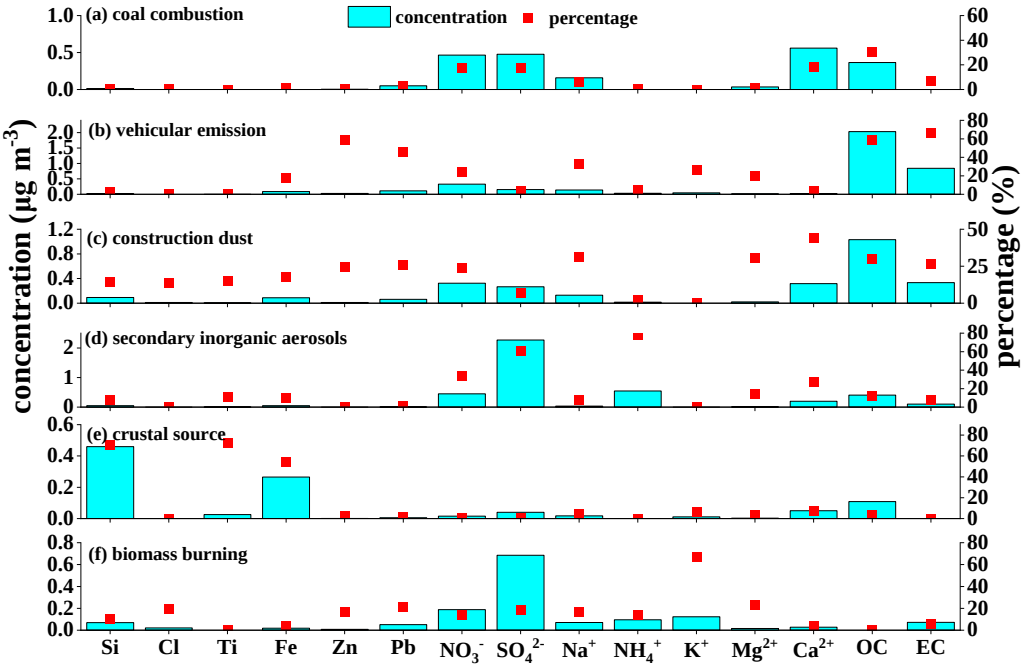

Figure S4. Source profiles of PMF for summer.

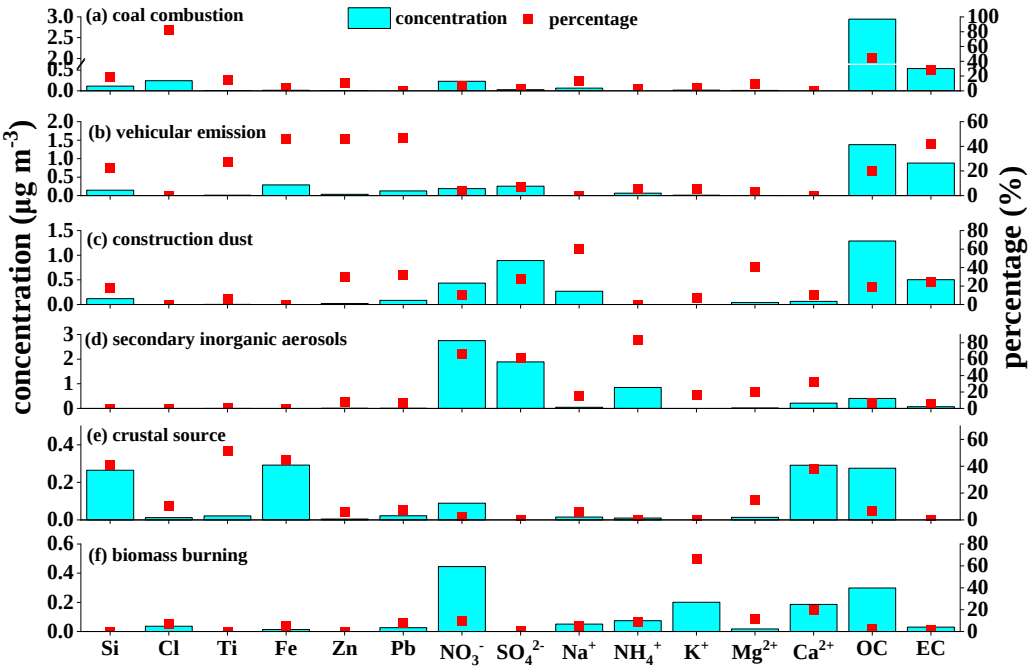

Figure S5. Source profiles of PMF for autumn.

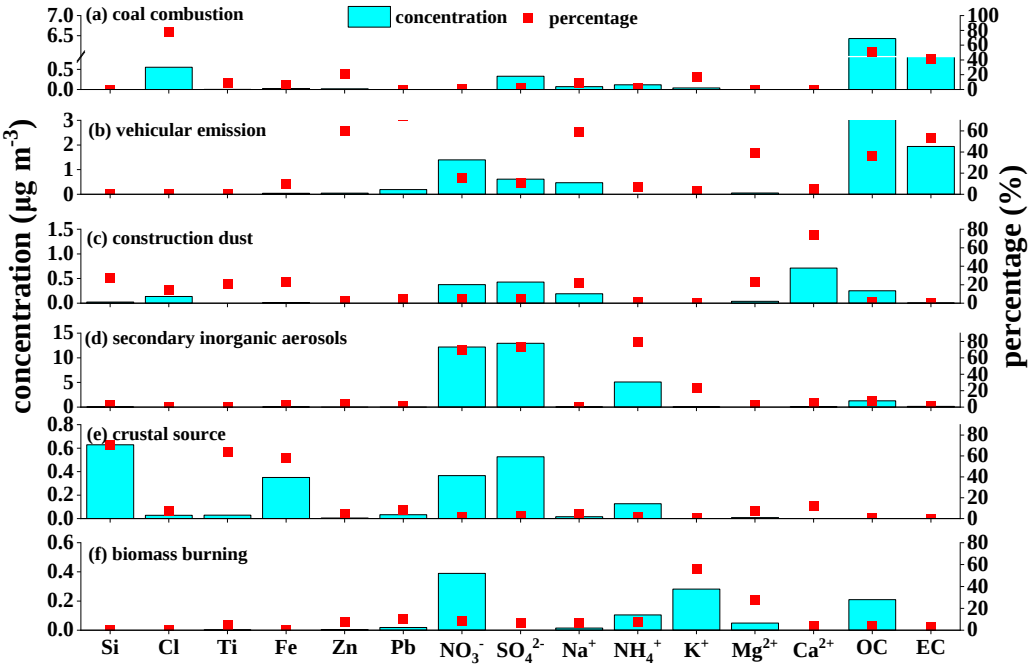

Figure S6. Source profiles of PMF for winter.

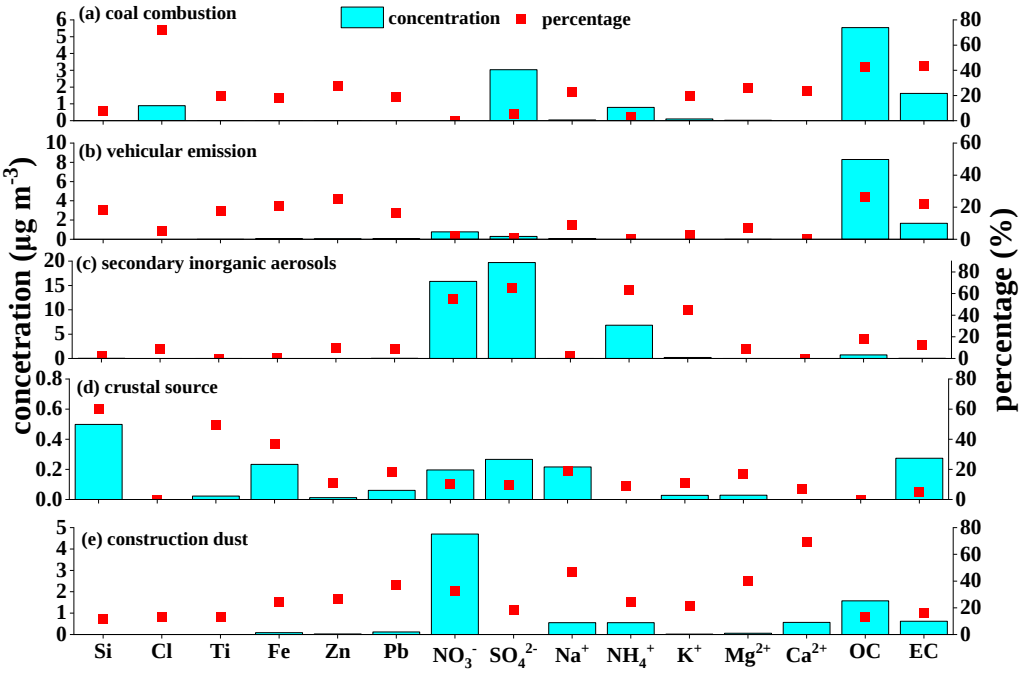

Figure S7. Source profiles of PMF during pre-lockdown.

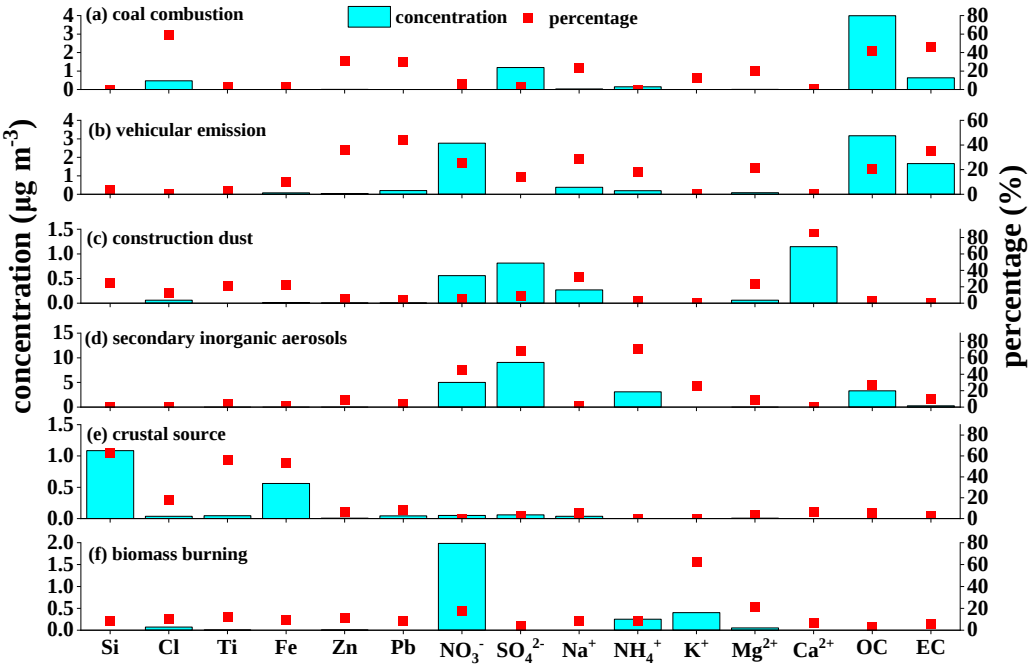

Figure S8. Source profiles of PMF during lockdown.

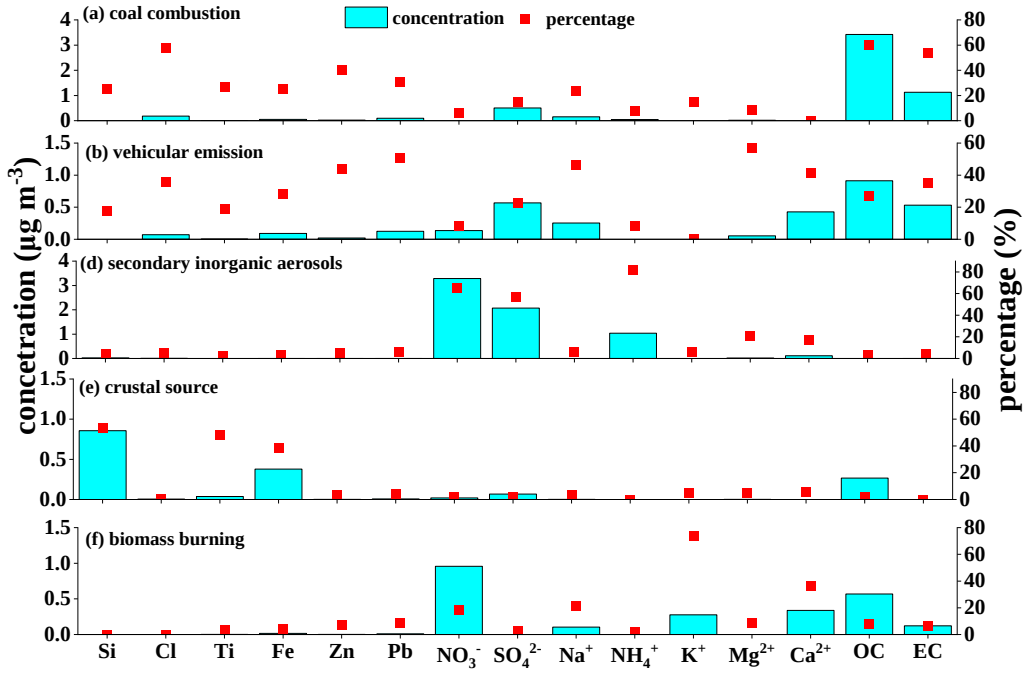

Figure S9. Source profiles of PMF during post-lockdown.

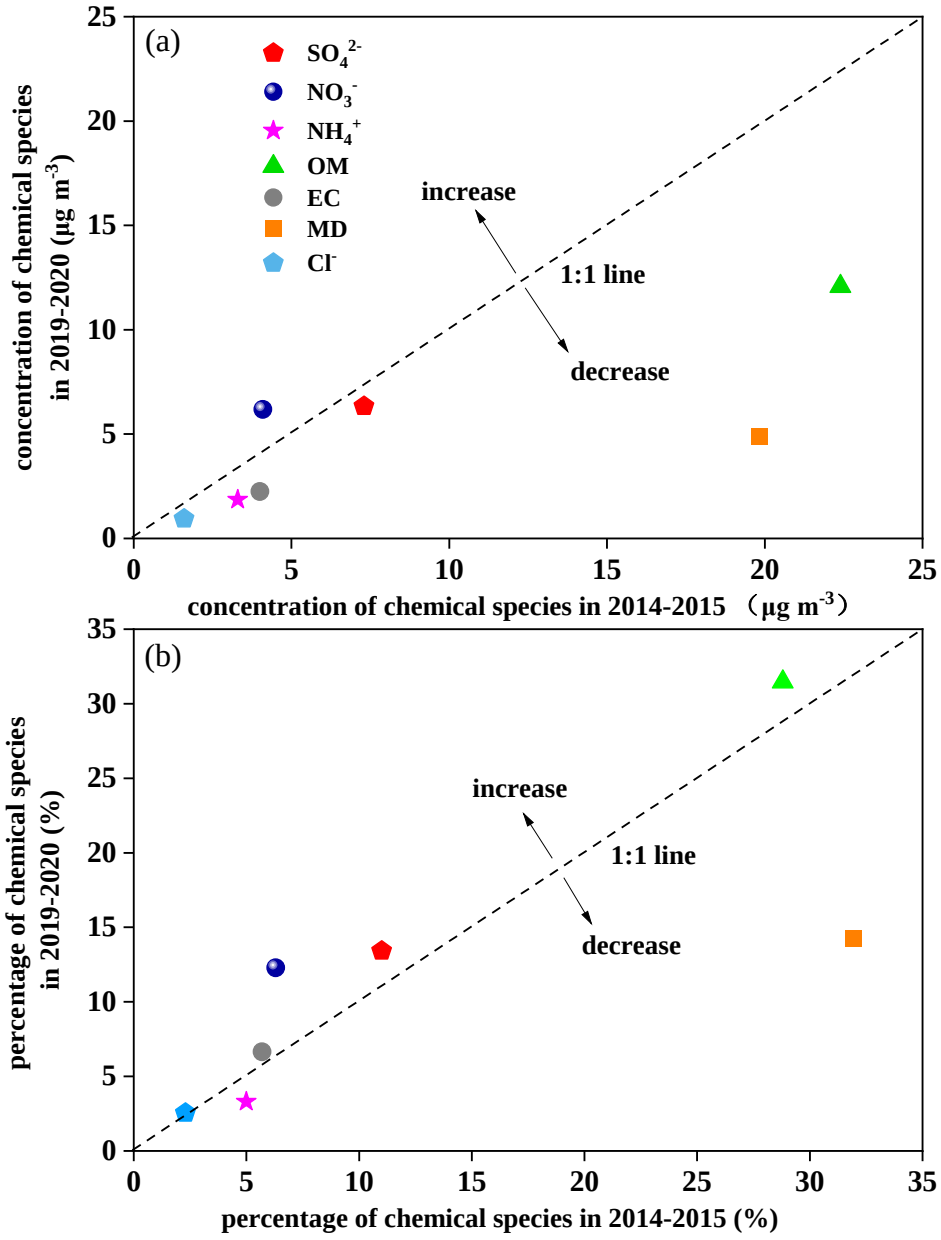

Figure S10. Comparation of chemical composition in (a) 2019-2020 and (b) 2014-2015 in Hohhot. The data of chemical composition in 2014-2015 were obtained from Wang (Wang et al., 2019). The organic matter (OM) and mineral dust (MD) were calculated by the following equations with the composition data, OM=1.6×[OC] and MD =2.14×[Si]+1.89×[Al]+1.40×[Ca]+1.43×[Fe] +1.58×[Mn] +1.21×[K]+1.67×[Ti].

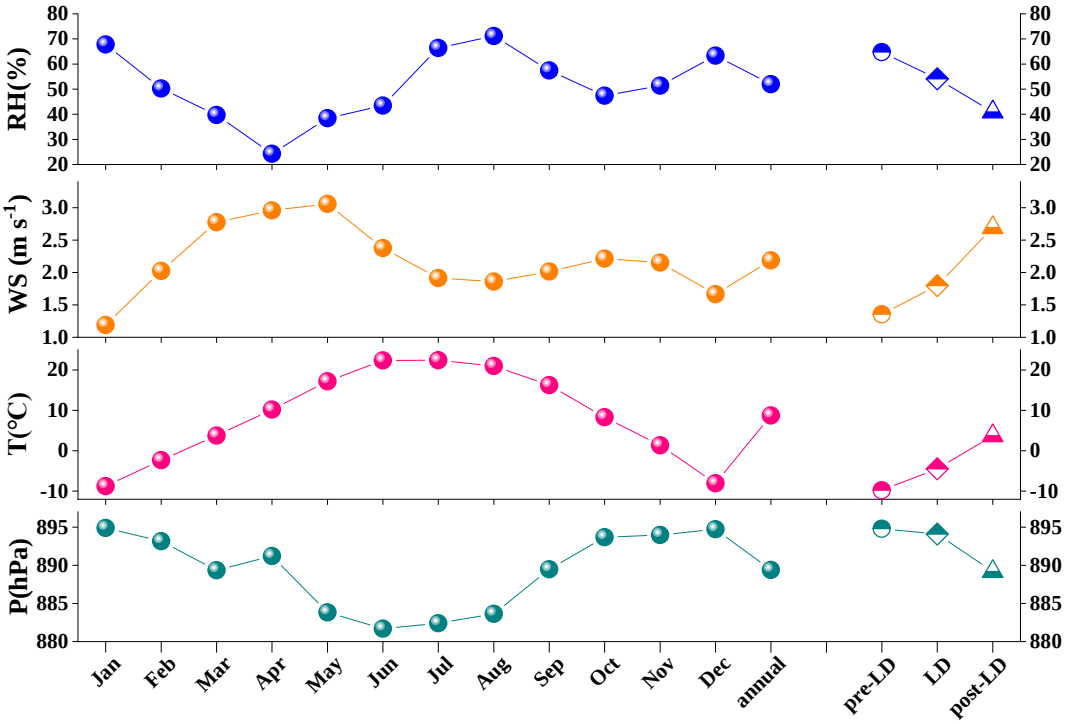

Figure S11. Monthly variation of (a) RH, (b) WS, (c) T, and (d) P in Hohhot during the sampling period.

References:

Chen, H., Huo, J., Fu, Q., Duan, Y., Xiao, H., and Chen, J.: Impact of quarantine measures on chemical compositions of $PM_{2.5}$ during the COVID-19 epidemic in Shanghai, China, Sci. Total Environ., 743, 140758, https://doi.org/10.1016/j.scitotenv.2020.140758, 2020.

Ding, J., Dai, Q., Li, Y., Han, S., Zhang, Y., and Feng, Y.: Impact of meteorological condition changes on air quality and particulate chemical composition during the COVID-19 lockdown, J. Environ. Sci.-China, 109, 45-56, https://doi.org/10.1016/j.jes.2021.02.022, 2021.

Feng, X., Feng, Y., Chen, Y., Cai, J., Li, Q., and Chen, J.: Source apportionment of $PM_{2.5}$ during haze episodes in Shanghai by the PMF model with PAHs, J. Clean. Prod., 330, 129850, https://doi.org/10.1016/j.jclepro.2021.129850, 2022.

Hong, Y., Xu, X., Liao, D., Zheng, R., Ji, X., Chen, Y., Xu, L., Li, M., Wang, H., Xiao, H., Choi, S.-D., and Chen, J.: Source apportionment of $PM_{2.5}$ and sulfate formation during the COVID-19 lockdown in a coastal city of southeast China, Environ. Pollut., 286, 117577, https://doi.org/10.1016/j.envpol.2021.117577, 2021.

Ren, C., Huang, X., Wang, Z., Sun, P., Chi, X., Ma, Y., Zhou, D., Huang, J., Xie, Y., Gao, J., and Ding, A.: Nonlinear response of nitrate to NOx reduction in China during the COVID-19 pandemic, Atmos. Environ., 264, 118715, https://doi.org/10.1016/j.atmosenv.2021.118715, 2021.

Tian, J., Wang, Q., Zhang, Y., Yan, M., Liu, H., Zhang, N., Ran, W., and Cao, J.: Impacts of primary emissions and secondary aerosol formation on air pollution in an urban area of China during the COVID-19 lockdown, Environ. Int., 150, 106426, https://doi.org/10.1016/j.envint.2021.106426, 2021.

Wang, H., Ding, J., Xu, J., Wen, J., Han, J., Wang, K., Shi, G., Feng, Y., Ivey, C. E., Wang, Y., Nenes, A., Zhao, Q., and Russell, A. G.: Aerosols in an arid environment: The role of aerosol water content, particulate acidity, precursors, and relative humidity on secondary inorganic aerosols, Sci. Total Environ., 646, 564-572, https://doi.org/10.1016/j.scitotenv.2018.07.321, 2019.

Wang, N., Xu, J., Pei, C., Tang, R., Zhou, D., Chen, Y., Li, M., Deng, X., Deng, T., Huang, X., and Ding, A.: Air quality during COVID-19 lockdown in the Yangtze River Delta and the Pearl River Delta: Two different responsive mechanisms to emission reductions in China, Environ. Sci. Technol., 55, 5721-5730, https://doi.org/10.1021/acs.est.0c08383, 2021.

Yumin, L., Shiyuan, L., Ling, H., Ziyi, L., Yonghui, Z., Li, L., Yangjun, W., and Kangjuan, L.: The casual effects of COVID-19 lockdown on air quality and short-term health impacts in China, Environ. Pollut., 290, 117988, https://doi.org/10.1016/j.envpol.2021.117988, 2021.

Z ková, N., Wang, Y., Yang, F., Li, X., Tian, M., and Hopke, P. K.: On the source contribution to Beijing $PM_{2.5}$ concentrations, Atmos. Environ., 134, 84-95, https://doi.org/10.1016/j.atmosenv.2016.03.047, 2016.